Applied Radiation and Isotopes 184 (2022) 110197

Contents lists available at ScienceDirect

Applied Radiation and Isotopes

journal homepage: www.elsevier.com/locate/apradiso

# Corrosion characterization of the 6061 Al–Mg–Si alloy in synthetic acid rain using neutron tomography

Mariana Xavier Milagre [a,*], Marco Stanojev Pereira [a], Antônio A. Gomes [a], Marcos Scapin [a], Margareth Franco [a], Fabiano Yokaichiya [b], Frederico Genezini [a], Isolda Costa [a]

[a] Instituto de Pesquisas Energéticas e Nucleares, IPEN/CNEN, Av. Prof. Lineu Prestes, 2242, São Paulo, Brazil
[b] Universidade Federal do Paraná, UFPR, Rua XV de Novembro, 1299, Curitiba, Brazil

ARTICLE INFO

*Keywords:*
Aluminum alloy
Localized corrosion
Exfoliation
3D optical profilometry
3D neutron tomography

ABSTRACT

Neutron tomography has gained increasing importance as an imaging technique for materials characterization. In general, neutron beams are able to show microstructure features of hydrogenous materials, even enfolded with thick metal layers. In the present paper, neutron tomography and observation of cross section images were successfully applied to investigate the corrosion features of the 6061 Al–Mg–Si alloy. The results showed good agreement between neutron 3D tomography and the cross section images obtained in the high attenuation areas of the samples, whereas significant differences in depth of corrosion penetration were obtained between the results from Neutron Tomography and 3D optical profilometry.

## 1. Introduction

The 6061 Al–Mg–Si alloy is applied in structural components of nuclear research reactors as cladding for nuclear fuel due to its high corrosion resistance when compared with Al alloys from other series and to its good radiation tolerance and compatibility with the primary coolant used in nuclear reactors (Howard et al., 2018).

The IEA-R1 is a pool type, light water moderate research reactor, localized at the Nuclear Research Institute (IPEN-CNEN) in São Paulo, Brazil. The IEA-R1 is the oldest research reactor in operation in South America. It operates using fuel plates containing $U_3Si_5$–Al dispersion type, with 20% enrichment of uranium fabricated at IPEN (Durazzo et al., 2019). The IEA-R1 fuel element consists of a 6061-T6 Al-alloy case with cladding also made of 6061 alloy covering the enriched nuclear fuel, as a "sandwich". In order to produce the fuel assembly, the "sandwich" is subjected to steps of heating and rolling. This process is known as Picture Frame Technique (PFT) (Durazzo et al., 2017, 2019).

The fuel plate assembly is composed of the U-enriched fuel concentrated in the "meat zone" surrounded by the 6061-PFT cladding. These plates are placed in a 6061-T6 case, which is processed by a commercial temper procedure including solubilization and artificial aging. The 6061-PFT alloy (cladding) presents different microstructure features from the 6061-T6 due to the thermomechanical conditions associated to PFT process affecting the corrosion behavior of the 6061 alloy (Milagre et al., 2020a, 2020b, 2020c).

The IEA-R1 nuclear reactor has been intensively used for research and production of primary radioisotopes used in the fabrication of radiopharmaceuticals for Nuclear Medicine (ATOMICA, 1958). The demand for these products increases each passing year. In the near future, for the safe continuity of the reactor operations, there will be a demand for wet storages and even final disposal facilities for the nuclear spent fuels.

The final disposal of the nuclear spent fuel comprises a high level of security operations in order to avoid any contact of the radioactive waste with the environment. The waste must be disposed in a multi engineering barrier repository. Each external barrier must guarantee the integrity of their subsequent inner layer to avoid damage of the fuel element and exposure of the irradiated material to the environment. Consequently, it is important to know and predict the corrosion behavior of the 6061 alloy for use in nuclear operations in different environments.

Previously results showed that the PFT process increases the corrosion resistance of the 6061 alloy by β'' (MgSi) phase dissolution, which is the strengthening phase in this alloy (Milagre et al., 2020b; ATOMICA, 1958). This phase chemical composition favors corrosion by preferential dissolution of Mg in acid/neutral solution and high alkaline environments (Eckermann et al., 2008a, 2008b).

Al alloys are susceptible to localized corrosion, therefore, the use of

* Corresponding author.
*E-mail address:* marianamilagre@yahoo.com.br (M.X. Milagre).

https://doi.org/10.1016/j.apradiso.2022.110197
Received 7 November 2021; Received in revised form 2 February 2022; Accepted 11 March 2022
Available online 24 March 2022

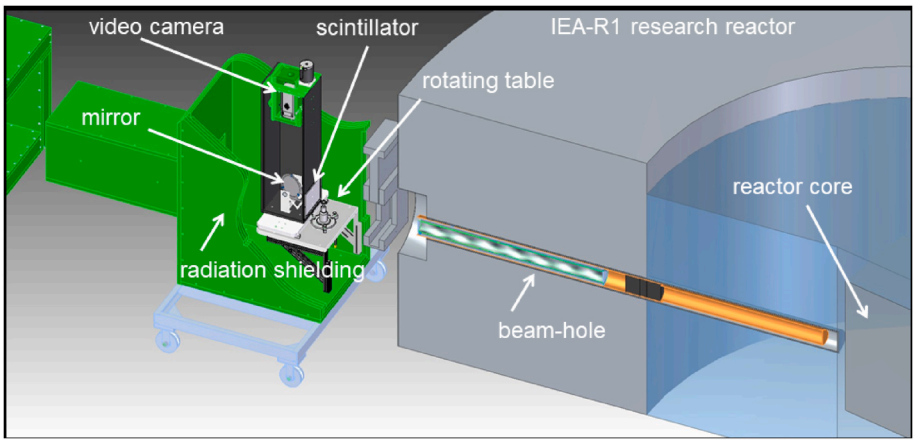


**Fig. 1.** Sketch of the equipment for neutron tomography.

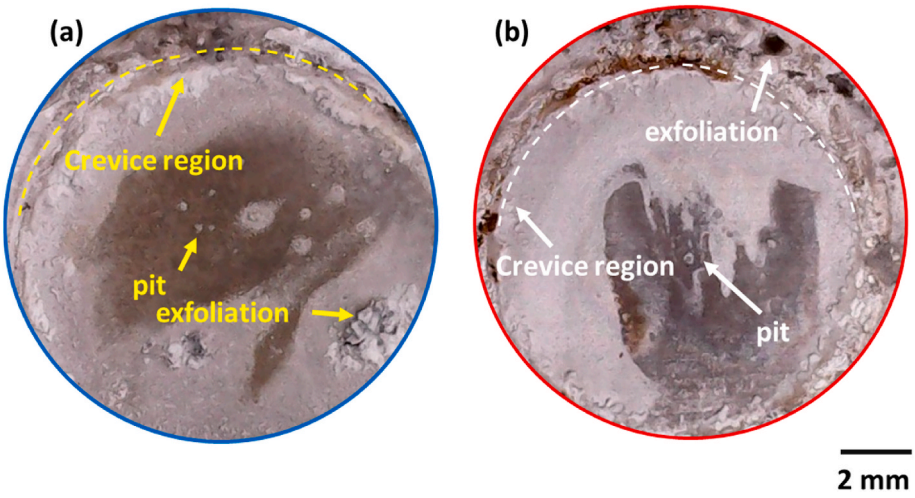


**Fig. 2.** Exposed surface of the 6061-PFT (a) and 6061-T6 alloy (b) after 30 days of immersion in synthetic acid rain solution.

techniques for detection and analysis of localized corrosion in order to prevent failures of Al alloys components in service is fundamental. Magnesium as alloying element in Al-alloys increases hydrogen solubility in the Al matrix because of its chemical affinity for hydrogen (Jones, 2003). According to Jones (Jones et al., 2001), increased β phase precipitation at the grain boundaries of the 5083 Al-alloy increases the alloy crack-growth rate since extensive hydrogen reduction occurs during anodic β phase dissolution process. Besides, alloying elements and heat treatments have been reported to influence hydrogen uptake in Al-alloys (Scamans and Tuck, 1979; Scamans et al., 1987).

Corrosion is associated with anodic reactions due to metal dissolution, and cathodic reactions with the main cathodic reactions consisting of either oxygen reduction, under aerated conditions, or hydrogen evolution, in acidic environments, Equations (1)–(3).

$$Al \rightarrow \ Al_{aq}^{3+} + 3e^{-} \quad (1)$$

$$O_2 + 2H_2O + 4e^{-} \rightarrow 4OH^{-} \quad (2)$$

$$2H + 2e^{-} \rightarrow \ H_2 \quad (3)$$

Hydrogen generation is associated with the corroded regions, mainly in highly aggressive environments. The hydrogen produced by reactions at the surface is initially chemically absorbed, but a continued exposure leads to buildup of absorbed hydrogen (Alexopoulos et al., 2019; Haidemenopoulos et al., 1998).

Neutron imaging techniques are a powerful tool employed to study the internal structure of an object. The applications of radiography (2D) and neutron tomography (3D) techniques cover several segments of science and industry. It is widely used in the analysis of components in the fields of aeronautics and aerospace; in the inspection of richly hydrogenated materials, even when encapsulated in some metals, such as steel, aluminum and lead; in the nuclear segment, in inspections of highly radioactive materials; in the health area for the study and development of biomaterials; in archeology as an archaeometric technique used in the study of restoration and conservation processes of historical and cultural heritage objects; and in materials engineering.

In this work, the localized corrosion of the 6061 Al alloy immersed in a synthetic acid rain solution was studied by imaging techniques such as Microscopy and 3D neutron tomography techniques. This last technique is a powerful nondestructive and non-invasive one, which allows detecting small quantities of hydrogen-rich substances, even when wrapped by thick metal layers (Dias et al., 1994; Taketani et al., 2017; Pfretzschner et al., 2019; Berger, 2004; Hawkesworth, 1977; Pugliesi et al., 1992). The results obtained were compared with cross-sectional observations of the immersed samples, and better agreement was obtained between cross-sectional images and 3D neutron tomography than between 3D optical profilometry and cross-sectional images.

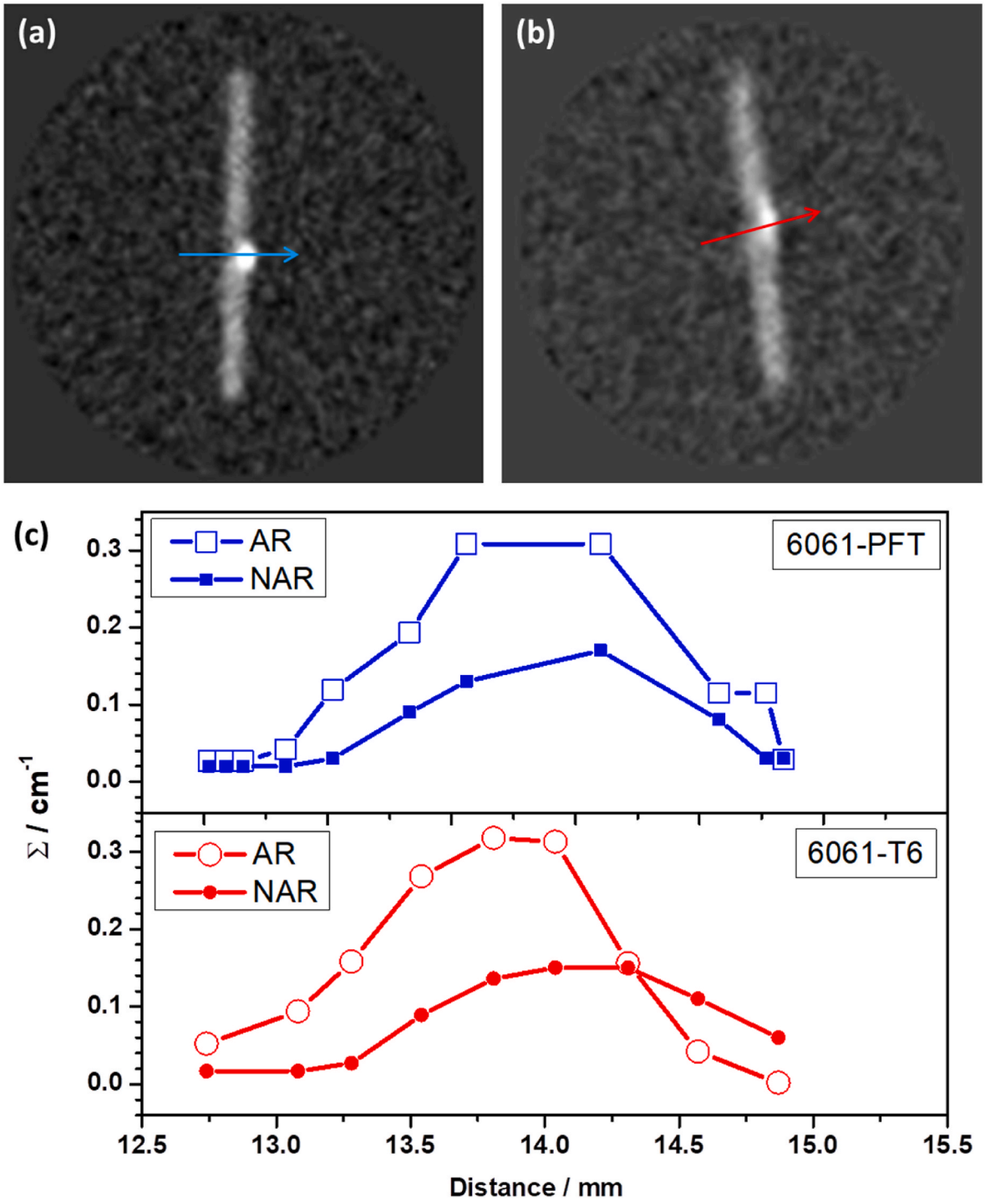


**Fig. 3.** Selected tomography corresponding to slices in the XY plane for the: (a) 6061-PFT and (b) 6061-T6 samples, after immersion for 30 days in synthetic acid rain solution. The arrows indicate the region of reading. (c) Distribution of the attenuation coefficient in the attacked region. AR = attacked region; ANR = non attacked region.

## 2. Experimental

### 2.1. Material

The 6061 alloy (Al 89.9 wt%, Cr 0.10 wt%, Cu 0.22%, Fe 0.20 wt%, Mg 0.90 wt%, Mn 0.05 wt%, Si 0.13 wt% and Zn 0.02 wt%), with (20 × 20 x 1.54) mm dimensions and different thermomechanical treatments was used in this study. The T6 temper is a commercial temper condition, whereas the PFT (Picture Frame Technique) is related to the nuclear fuel cladding manufacturing process.

### 2.2. Immersion test

The surface of the samples for exposure to the test solution was sequentially ground with SiC emery papers (#500, #800, #1200, #2500, #4000). Subsequently, the samples were immersed in 40% NaOH solution at 60 °C for 1 min and then in 30% $HNO_3$ solution for 1 min. Finally, the samples were rinsed in deionized water and dried.

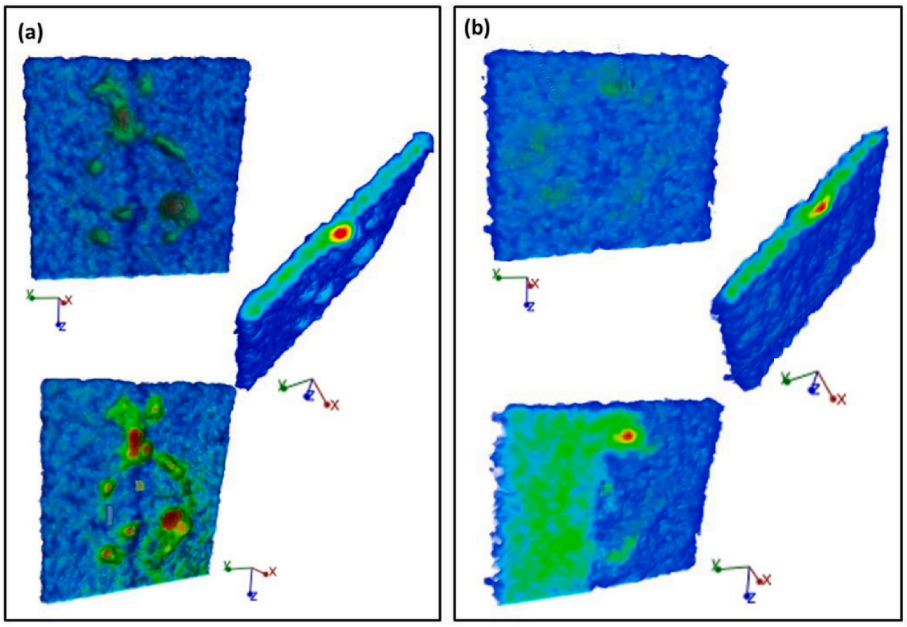


**Figs. 4.** 3D neutron tomography of the 6061-PFT (a) and 6061-T6 (b) samples after 30 days of immersion in synthetic acid rain solution.

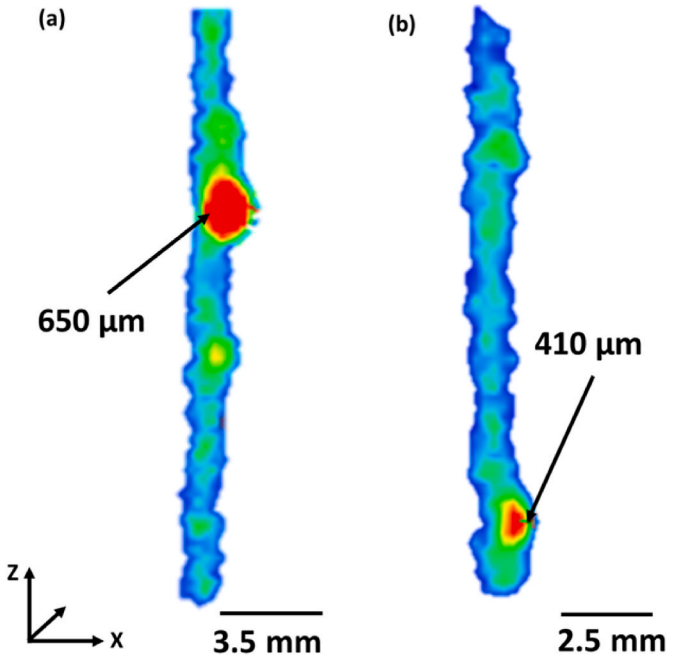


**Figs. 5.** 3D profile images of the samples showing the extent of damage caused by the action of acid in the (a) 6061-PFT and b) 6061-T6 alloys.

Later, the samples were immersed for 30 days in a synthetic acid rain solution composed of 3.91 g $L^{-1}$ $CaCl_2$, 1.82 g $L^{-1}$ $(NH_4)_2SO_4$, 1.77 g $L^{-1}$ $Na_2SO_4$, 1.81 g $L^{-1}$ $NaNO_3$, 0.69 g $L^{-1}$ $NaHCO_3$ and $H_2SO_4$, with pH adjusted to 4.5.

### 2.3. Microscopy techniques

The exposed surface was examined by Optical Microscopy (OM) and to characterize corrosion morphology and penetration, a Scanning Electron Microscope (SEM) (Hitachi TM 30000 with an incident beam of 15 keV.

### 2.4. 3D optical profilometry

ZYGO's ZeGage™ 3D optical profilometer was used in order to analyze the corroded surfaces. The 3D optical profilometer technique is based on the coherence scanning interferometry, which uses white light to measure the height on a surface. A light source directs the white light through the interference objective and the beam is split by a beam splitter. Part of the beam is reflected to the sample and part to a very smooth reference mirror (with a known roughness), inside the objective. The signals are, thus, recombined by a detector. However, they are susceptible to constructive or destructive interferences. These constructive or destructive interferences will generate fringes which are captured by the camera. These fringes with different gray scales are related to the different heights over the sample surface.

### 2.5. Neutron tomography

The equipment for Neutron Tomography is installed at the Beam - Hole (BH) #14, of the 5 MW IEA - R1 Nuclear Research Reactor, of the IPEN - CNEN/SP. Fig. 1 shows the equipment sketch, and some of its main components are: the rotating table where the sample to be studied is irradiated; the scintillator screen ($Li^6F$/ZnS - NE426) where the image of the internal structure of the sample is formed; the plane mirror that reflects this image to the video camera; the CCD video camera (ANDOR Ikon – M, 16 bits, 1024 × 1024 pixels, 12 × 12 $\mu m^2$ pixel size) for imaging capture; the radiation shielding. The camera and the rotating table are coupled to a computer that is, it is automated in such a way that after the first image is captured, the sample is rotated and a new image is taken. The rotating table is able to rotate the sample between 0 and $360^0$. At present, 400 images are necessary for a tomography. The angle between images is $0.9^0$ and the time per image capture is 1s. The Octopus V8.7 software was employed for image reconstruction in the planes XY, XZ, YZ, and the VGStudioMAX V2.2 software was used for 3D visualization. The neutron flux at the irradiation position (measured by the Au - foil method) was $8 \times 10^6$ n $cm^{-2}$ $s^{-1}$, the flat field of the beam is 16 cm in diameter. The best spatial resolution is (205 ± 25) µm (Pugliesi et al., 2017), and the field of view is 18 × 18 $cm^2$. The references (Schoueri et al., 2014; Pugliesi et al., 2019; Ugliesi et al., 2014) describe in detail the equipment and the procedures for tomography.

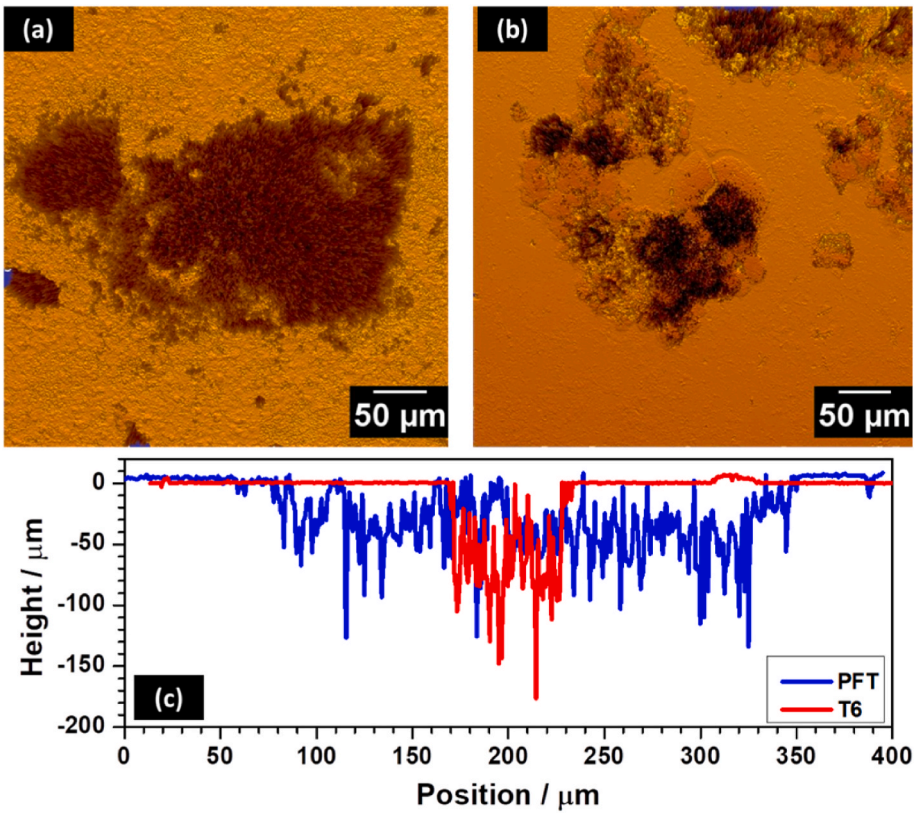


**Figs. 6.** 3D optical profilometer images of the (a) 6061-PFT and (b) 6061-T6 samples after 30 days of immersion in synthetic acid rain solution; (c) depth of attacked areas and surroundings.

## 3. Results and discussion

Fig. 2 shows the surface of the 6061-PFT (Figs. 2a) and 6061-T6 (Fig. 2b) after immersion test. The condition of immersion favored the development of a high aggressive environment which favored pitting, exfoliation and crevice corrosion, indicated by arrows.

After immersion test, the samples were irradiated in the neutron beam to acquire the 2D image file. After reconstruction process, a file containing several images was obtained, each one corresponding to a slice referring to the XY visualization plane. Each slice refers to a thickness of 0.28 mm of the sample.

Fig. 3a–b shows one of the slices from the reconstructed images file. The images illustrate the potential for qualitative and quantitative analysis of the neutron tomography technique. It is worthwhile to mention that, as a first analysis of the tomography slices, areas of different neutron attenuation can be clearly identified. The brighter the area, the higher the attenuation. These areas could be related to humidity and/or corrosion products. The attenuation coefficient in the sample was estimated using the Octopus 8.7 software by the pixel by pixel reading between the interface of the lowest brightness regions to the highest ones. Quantification was carried out by scanning the pixels as a function of scan along the x-axis, that corresponds to the thickness of the sample. As it can be observed in Fig. 3c, at the regions of highest brightness, the values of attenuation coefficient are different in the 6061 matrix, for both alloys. At the peak, the values are about 0.30 $cm^{-1}$, whereas at the intact region, the values are inferior to 0.05 $cm^{-1}$.

In order to complement the study, Fig. 4 shows selected and processed 3D images of the inspected samples obtained by means of the software VGStudio Max 2.2.

The blue regions represent those of highest transmission whereas those of highest attenuation are indicated by yellow and red colors. For the 6061-PFT sample (Fig. 4a), the highest attenuation sites are related to the regions that suffered exfoliation, indicated by white arrows in Fig. 2a. On the other hand, for the 6061-T6 sample (Fig. 4b), a small area of high attenuation was observed and this was related to pits indicated by the white arrows in Fig. 2b.

Fig. 5 displays the area of greatest attenuation (red) and it shows that the affected area is corresponding to a total thickness of 650 μm, for the PFT, and 410 μm, for the T6 temper condition.

These results were compared with 3D optical profilometry analysis, Fig. 6, which has the advantage of being a non-destructive method of analysis. The regions of highest attenuation in Figs. 3 and 4 correspond to those of reduced penetration depth when analyzed by optical profilometry. For the PFT sample, depths of penetration around 140 μm were related to the corroded (pits) region, whereas for the T6 condition, depths of about 180 μm were observed. Accelerated test conditions are too detrimental to Al alloys, especially for the PFT condition which has shown higher corrosion resistance in previous works (Milagre et al., 2020a, 2020c).

During profilometry analysis it is the z axis that varies. Thus, the focused region of the sample also varies. As the technique is based on fringes intensity, it is limited to the light capability to penetrate through the material, with the high intensity signal being reflected to the detector. For this reason, interferometry (WLI) is advantageous for smooth surfaces. If the sample is rough or, corroded, the technique is limited. Also, the deposition of corrosion products inside the pits affects the accuracy of pits depth measurement. For these reasons, different values of localized corrosion penetration are observed when compared with neutron tomography images. These results showed the need to use complementary techniques to 3D profilometry in order to analyze pit penetration. Fig. 7 shows top surfaces and cross-section micrographs images corresponding to the high attenuation regions showed in Fig. 5.

The cross-section images showed in Fig. 7 are in agreement with the results obtained in Fig. 5. The aluminum alloys employed is this study are materials of very low neutron attenuation coefficient (Reillo et al., 2008), and this transparency, associated with the oxidation reaction

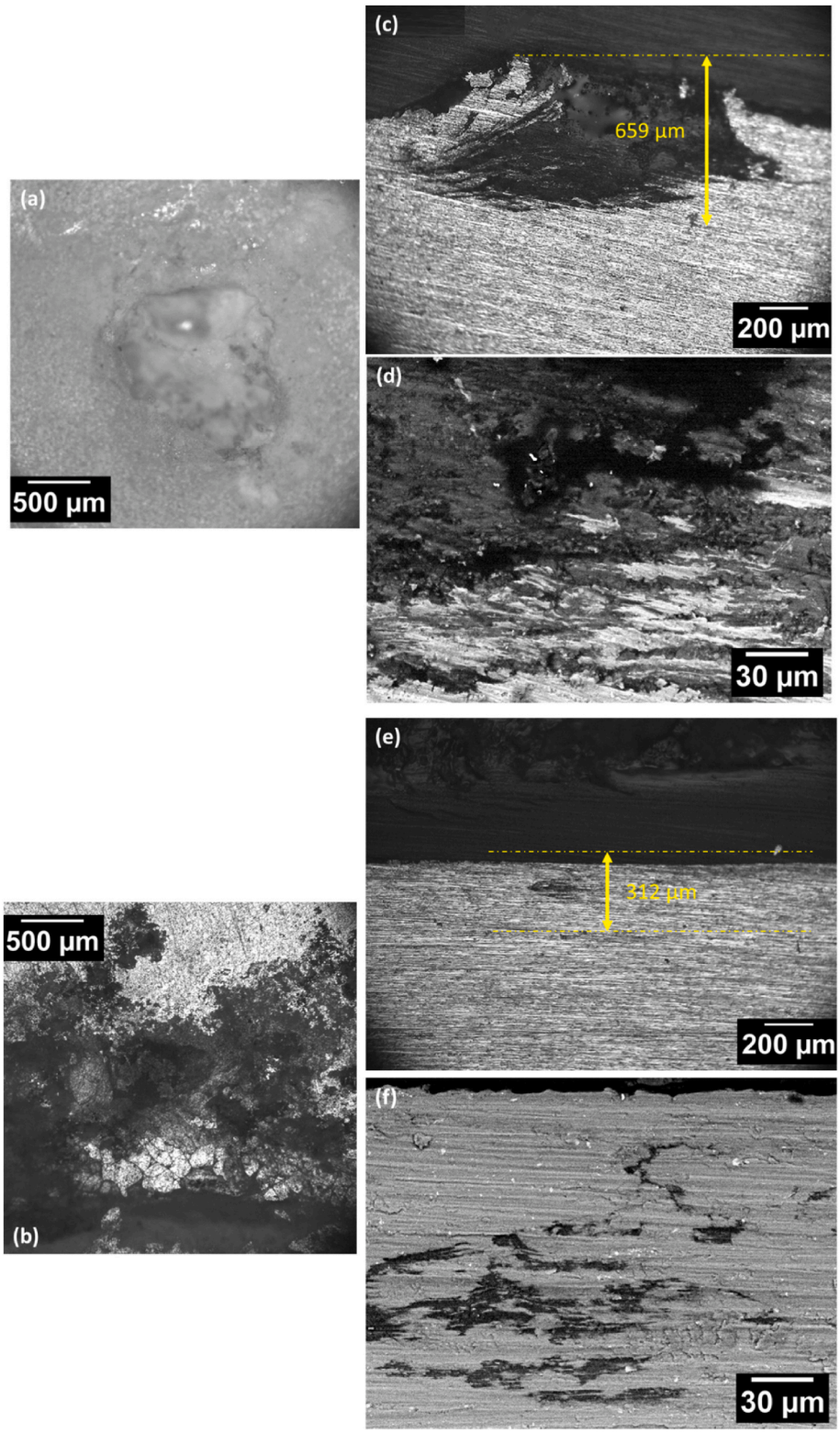


**Fig. 7.** Top-surface micrograph images of areas in the 6061-PFT related to (a) exfoliation and (b) pitting in the 6061-T6 after 30 days of immersion in synthetic rain solution. Cross-sections of the regions (c–d) showed in (a); and (e–f) showed in (b).

products, that present high attenuation coefficient, results in images of great contrast. As the neutron tomography technique uses an algorithm to reconstruct a set of radiographic projections, the images obtained have different gray scales which are dependent on the attenuation coefficient of the sample (Zanarini et al., 1995) allowing the analysis of the samples volume. In the 3D images (Figs. 4 and 5), oxidation reaction products contents are related to bright regions because the algorithm for reconstruction of the images calculates the attenuation coefficient using the transmitted intensity for every captured pixel. Hence, high attenuation coefficients are displayed as bright pixels, and the location of the intense scattering is shown (Pfretzschner et al., 2019). The high transparency of the metal and the high attenuation of the corroded areas

seemingly allow a more precise evaluation of pits depth comparatively to the cross section method. The high agreement obtained for the PFT alloy can be related to the propagation of corrosion. The largest area of the exfoliation blister (Fig. 7a) and the deep intragranular attack Fig. 7 (c–d) were observable by the "naked eye" allowing the accurate choice of the area for cross section preparation in order to analyze the localized attack penetration. However, for the T6 alloy (Fig. 7b) the small "pit mouth" and the thin nature of intergranular attack, made it difficult to metallographically prepare the samples in the cross section. As it can be observed in Fig. 7e–f, depth information was lost during sample grinding, which is dependent on the operator ability. The results showed the advantages of using neutron tomography and radiography technique as complementary techniques for 3D profilometry or cross-section images. The two last techniques are common techniques to evaluate pit penetration of Al-alloys, however they have disadvantages when used in isolation. As previously discussed, depending on the morphology of the attack, the light access is difficult into the material, and as consequence, focus necessary to generate the optical profilometry images becomes difficult. In the same way, thin regions of attack can be lost during the cross section samples preparation. Due to the highest transparency of Al to neutrons beam, the regions of highest attenuation, for instance, the corroded areas with deepest penetration, are easily identified.

## 4. Conclusions

The neutron radiography (2D) and neutron tomography (3D) techniques were used in the present study as nondestructive and noninvasive methods to provide information on the pits depth in Al 6061 alloys. Together with Optical Microscopy techniques (OM), Scanning Electron Microscope (SEM) and Optical 3D Profilometer, it was possible to study and quantify the damage caused by induced oxidation on the metal surface, using the tools available in digital image processing and analysis software employed. The regions of deepest pit penetration, precise prevision of pit growth rates can be performed by the use of neutron radiography (2D) and neutron tomography (3D) techniques. The results obtained corroborate with monitoring of the alloys by cross section observation and avoids the loss of information which might occur during analysis of small and thin pits by cross section observations. Roughness and deposition of corrosion products in the corroded areas were drawbacks for a good agreement between the 3D optical profilometer measurements and the other techniques. Finally, accelerated tests highlighted the harmful effects of exposing the 6061 alloy to acid environments favoring exfoliation and pitting of the alloy that is used in assemblies applied in nuclear fuel reactors.

## CRediT authorship contribution statement

**Mariana Xavier Milagre:** Writing – original draft, Conceptualization. **Marco Stanojev Pereira:** Software, Writing – review & editing. **Antônio A. Gomes:** Software, Writing – review & editing. **Marcos Scapin:** Writing – review & editing, Supervision. **Margareth Franco:** Supervision, Writing – review & editing. **Fabiano Yokaichiya:** Writing – review & editing, Supervision. **Frederico Genezini:** Supervision, Writing – review & editing. **Isolda Costa:** Writing – review & editing, Supervision, Funding acquisition.

## Declaration of competing interest

The authors declare that they have no known competing financial interests or personal relationships that could have appeared to influence the work reported in this paper.

## Acknowledgments

The authors acknowledge the National Commission for Nuclear Energy (CNEN) and the Nuclear and Energy Research Institute (IPEN/CNEN-SP) in Brazil for financial support to this work and for the grant of Mariana X. Milagre (SEI 01342.002357/2019-32). Acknowledgements are due Dr. Wagner de Rossi from the Center of Lasers and Applications (CLA) of the Nuclear and Energy Research Institute (IPEN/CNEN-SP) for technical support with 3D profilometry analysis.

## References

Alexopoulos, N.D., Siskou, N., Charalampidou, C.M., Kourkoulis, S.K., 2019. Simulation of the corrosion-induced damage on aluminum alloy 2024 specimens with equivalent surface notches. Frat. Ed. Integrità Strutt. 13, 342–353. https://doi.org/10.3221/IGF-ESIS.50.29.

Atomica, I. de E., 1958. RADIOISÓTOPOS ARTIFICIAIS PREPARADOS COM O REATOR I E A R-1.

Berger, H., 2004. Advances in neutron radiographic techniques and applications: a method for nondestructive testing. Appl. Radiat. Isot. 61, 437–442. https://doi.org/10.1016/j.apradiso.2004.03.066.

Dias, A.F., Araújo, A.D.A., Crispim, V.R., 1994. Aluminum corrosion detection by using a neutron radiographic image analyzer. Proc. - Int. Conf. Image Process. ICIP. 2, 316–320. https://doi.org/10.1109/ICIP.1994.413583.

Durazzo, M., Souza, J.A.B., de Carvalho, E.F.U., Riella, H.G., 2017. Effect of porosity on the manufacturing of U3O8-Al dispersion fuel plates. Prog. Nucl. Energy 99, 49–58. https://doi.org/10.1016/j.pnucene.2017.05.001.

Durazzo, M., Umbehaun, P.E., Torres, W.M., Souza, J.A.B., Silva, D.G., Andrade, D.A., 2019. Procedures for manufacturing an instrumented nuclear fuel element. Prog. Nucl. Energy 113, 166–174. https://doi.org/10.1016/j.pnucene.2019.01.021.

Eckermann, F., Suter, T., Uggowitzer, P.J., Afseth, A., Schmutz, P., 2008a. The influence of MgSi particle reactivity and dissolution processes on corrosion in Al-Mg-Si alloys. Electrochim. Acta 54, 844–855. https://doi.org/10.1016/j.electacta.2008.05.078.

Eckermann, F., Suter, T., Uggowitzer, P.J., Afseth, A., Stampanoni, M., Marone, F., Schmutz, P., 2008b. Electrochemically controlled corrosion initiation and propagation in AlMgSi alloys in-situ monitored using X-ray. Microtomography 11, 23–38. https://doi.org/10.1149/1.2925260.

Haidemenopoulos, G.N., Hassiotis, N., Papapolymerou, G., Bontozoglou, V., 1998. Hydrogen absorption into aluminum alloy 2024-T3 during exfoliation and alternate immersion testing. Corrosion 54, 73–78. https://doi.org/10.5006/1.3284830.

Hawkesworth, M.R., 1977. Neutron radiography. Equipment and methods. At. Energy Rev. 15, 169–220.

Howard, R.H., Gallagher, R.C., Field, K.G., 2018. Mechanical performance of neutron-irradiated dissimilar transition joints of aluminum alloy 6061-T6 and 304L stainless steel. J. Nucl. Mater. 508, 348–353. https://doi.org/10.1016/j.jnucmat.2018.05.070.

Jones, R.H., 2003. The influence of hydrogen on the stress-corrosion cracking of low-strength Al-Mg alloys. JOM (J. Occup. Med.) 55, 42–46. https://doi.org/10.1007/s11837-003-0225-5.

Jones, R.H., Baer, D.R., Danielson, M.J., Vetrano, J.S., 2001. Role of Mg in the stress corrosion cracking of an Al-Mg alloy. Metall. Mater. Trans. A Phys. Metall. Mater. Sci. 32, 1699–1711. https://doi.org/10.1007/s11661-001-0148-0.

Milagre, M.X., Donatus, U., Maria, R., Silva, P., Victor, J., Araujo, S., Souto, R.M., Costa, I., 2020a. Galvanic coupling effects on the corrosion behavior of the 6061 aluminum alloy used in research nuclear reactors. J. Nucl. Mater. 541, 152440. https://doi.org/10.1016/j.jnucmat.2020.152440.

Milagre, M.X., Franco, M., Genezini, F., Wimpory, R.C., Yokaichiya, F., Costa, I., 2020b. A correlation between microstructure and residual stress in the 6061 Al–Mg–Si alloy with different thermomechanical process. SN Appl. Sci. 2, 1–9. https://doi.org/10.1007/s42452-020-03945-y.

Milagre, M.X., Donatus, U., Mogili, N.V., Machado, C.S.C., Araujo, J.V.S., Klumpp, R.E., Fernandes, S.M.C., de Souza, J.A.B., Costa, I., 2020c. Effects of picture frame technique (PFT) on the corrosion behavior of 6061 aluminum alloy. J. Nucl. Mater. 539, 152320.

Pfretzschner, B., Schaupp, T., Griesche, A., 2019. Hydrogen in metals visualized by neutron imaging. Corrosion 75, 903–910. https://doi.org/10.5006/3104.

Pugliesi, R., de Menezes, M.O., Assunção, M.P.M., 1992. Detection of aluminum corrosion products by neutron radiography. Int. J. Radiat. Appl. Instrumentation. Part. 43, 663–665. https://doi.org/10.1016/0883-2889(92)90037-F.

Pugliesi, R., Pereira, M.A.S., Schoueri, R.M., 2017. Method to evaluate the L/D ratio of neutron imaging beams. Braz. J. Radiat. Sci 1–7, 05–01.

Pugliesi, R., Pereira, M.A.S., Andrade, M.L.G., Basso, J.M.L., Voltani, C.G., Gonzales, I.C., 2019. Study of the fish fossil notelops brama from araripe-basin Brazil by neutron tomography. Nucl. Instruments Methods Phys. Res. Sect. A Accel. Spectrometers, Detect. Assoc. Equip. 919, 68–72. https://doi.org/10.1016/j.nima.2018.12.001.

Reillo, E., Martínez, T., Mendoza, E., 2008. On the neutron transparency of various materials proposed for the AIDA enclosure. In: AIDA Meet. - STFC RAL. https://www2.ph.ed.ac.uk/~td/AIDA/Meetings/12May2008/AIDA_chamber.pdf.

Scamans, G.M., Tuck, C.D.S., 1979. Embrittlement of aluminium alloys exposed to water vapour. In: Proc. Symp. Environ. Fract. Eng. Mater. Metallurgical Sociaty AIME, New York, pp. 464–483.

Scamans, G.M., Holroyd, N.J.H., Tuck, C.D.S., 1987. The role of magnesium segregation in the intergranular stress corrosion cracking of aluminum alloys. Corrosion Sci. 27, 329–347.

Schoueri, R.M., Domienikan, C., de Toledo, F., Andrade, M.L.G., Stanojev Pereira, M.A., Pugliesi, R., 2014. The new facility for neutron tomography of IPEN-CNEN/SP and its potential to investigate hydrogenous substances. Appl. Radiat. Isot. 84, 22–26. https://doi.org/10.1016/j.apradiso.2013.10.019.

Taketani, A., Yamada, M., Ikeda, Y., Hashiguchi, T., Sunaga, H., Wakabayashi, Y., Ashigai, S., Takamura, M., Mihara, S., Yanagimachi, S., Otake, Y., Wakabayashi, T., Kono, K., Nakayama, T., 2017. Visualization of water in corroded region of painted steels at a compact neutron source. ISIJ Int. 57, 155–161. https://doi.org/10.2355/isijinternational.ISIJINT-2016-448.

Ugliesi, R.P., Ndrade, M.L.G.A., Ereira, M.A.S.P., Choueri, R.M.S., Ias, M.S.D., 2014. Scientific Reviews Neutron imaging at the IPEN-CNEN/SP and its use in technology. Neutron News 25, 40–44.

Zanarini, M., Chirco, P., Rossi, M., Baldazzi, G., Guidi, G., Querzola, E., Scannavini, M.G., Casali, F., Garagnani, A., Festinesi, A., 1995. Evaluation of hydrogen content in metallic samples by neutron computed tomography. IEEE Trans. Nucl. Sci. 42, 580–584. https://doi.org/10.1109/23.467910.